Impact of soil temperature-difference on desert carbon-sink

F. Yang[1, 2], J. P. Huang[2, 3]†, Q. He[1], C. L. Zhou[1], H. L. Pan[1], W. Huo[1], X. Q. Zheng[4], H. P. Yu[3], X. Y. Liu[3], L. Meng[1], D. L. Han[2], M. Ali[1], and X. H. Yang[1]

[1]Taklimakan Desert Meteorology Field Experiment Station of CMA, Institute of Desert Meteorology, China Meteorological Administration, Urumqi, China.

[2]College of Atmospheric Sciences, Lanzhou University, Lanzhou, China.

[3]Collaborative Innovation Center for Western Ecological Safety, Lanzhou University, Lanzhou, China.

[4]Xinjiang Agro-Meteorological Observatory, Urumqi, China.

† Corresponding author: Jianping Huang (email: hjp@lzu.edu.cn)

Collaborative Innovation Center for Western Ecological Safety, Lanzhou University, Lanzhou, China, 730000

Key Points:

- Taklimakan Desert shifting sand play the role of a stable carbon-sink with a CO_2 annual uptake of 1.60×10^6 $t\cdot a^{-1}$.
- The shifting desert CO_2 exchange is dominated by the soil air expansion/contraction and salts/alkalis chemistry.
- The increase of soil temperature-difference will cause the carbon-sink decrease in the Taklimakan Desert.

Abstract

The global carbon-cycle is crucial for climate change. Desert, which has long been neglected in the global carbon-cycle, may sequester enormous volumes of CO_2 and play the role of a carbon-sink. As the world's second-largest shifting desert, the Taklimakan Desert (TD) contributes substantially to desert carbon-sinks. However, the contributions of the internal processes of the TD to its carbon-sink and the long-term trend of the carbon-sink under climate change are still unclear. This study will address this important knowledge gap. Through field observations, we found that the expansion/contraction of soil air containing CO_2 caused by heat fluctuation in shifting sand, in combination with salts/alkali chemistry dominates the release/absorption processes of CO_2 in shifting sand. The mutual counteraction of these processes means that the TD shifting sand acts as a stable carbon-sink that had a CO_2 annual uptake of 1.60×10^6 $t\cdot a^{-1}$ during 2004–2017. It suggests that global shifting deserts maybe uptake of ~2.125×10^8 t of CO_2 per year. However, an increasing soil temperature-difference will stimulate soil air expansion of desert and release more CO_2 into the atmosphere under climate change, causing the shifting sand carbon-sink decrease in the TD gradually in the future. These processes will be accelerated by positive feedback effect under climate change and enhance regional warming. These conclusions are very important for re-recognizing the status of deserts in the carbon-cycle, narrowing the gap in the missing carbon-sink and assessing the global carbon-cycle.

1 Introduction

The main carbon pool in a terrestrial ecosystem is soil (Post et al., 1982; Jobbagy and Jackson, 2000), among which the gross reserves of carbon are ~1500 Pg (1 Pg = 1015 g) (Batjes, 1996). The estimated amount of carbon released worldwide from the soil into the atmosphere is 77 Pg annually (Raich and Potter, 1995), which is the major routes for carbon to enter the atmosphere from soil (Singh and Gupta, 1977; Schlesinger and Andrews, 2000; Lou and Zhou, 2006). Even slight variations in this process can have far-reaching effects on the atmospheric CO_2 concentration, and could facilitate a positive feedback effect with climatic change (Houghton et al., 1998; Rustad et al., 2000; Friedlingstein et al., 2001; Han et al., 2018). Meanwhile, this process has been used to characterise a variety of ecosystem processes and properties, including soil C turnover, the functional role of differing origins of organic matter supporting C cycling, and biotic distribution and activity (e.g. Burkins et al., 2001; Barrett et al., 2006; Hopkins et al., 2006; Li et al. 2018). Therefore, it is crucial to understand soil CO_2 flux in different regions for accurate assessment of regional and global carbon cycle, and formulation of climate change countermeasures.

Soil CO_2 flux is extremely sensitive to environmental changes and is usually affected by a combination of soil biological and abiologic processes. In ecosystems with relatively high productivity, the biological processes are very active, and the effects of abiologic processes (such as soil temperature gradient, soil moisture content, soil parent material, etc) on soil CO_2 flux are often ignored (Parsons et al. 2004). However, in extreme environments of relatively low productivity with low temperatures, drought, extreme deficiency of biological resources, etc., the biological processes are relatively sluggish, and the effects of abiologic processes on soil CO_2 flux cannot be completely ignored although soil CO_2 flux is extremely weak. In such an extreme environment, the effect of biological processes are even smaller than that of abiotic processes (Parsons et al. 2004; Shanhun et al. 2012). Abiologic processes generally affect soil CO_2 flux by changing CO_2 dissolution, adsorption, carbonate dissolution/precipitation, and chemical oxidation of carbon-containing compounds in soil. They also simultaneously affect the diversity, quantity, and activity of soil microorganisms (Barrett et al. 2006 and 2008).

Desert ecosystem, as a typical extreme environment widely distributed, has been widely concerned by the scientific community in recent years due to the discovery that it can store a lot of CO_2 and reduce the missing carbon-sink. By continuously conducting in-depth research on, it was gradually found that soil CO_2 flux in deserts is closely related to abiologic processes (such as soil temperature gradient, soil moisture content, soil parent material, soil pH, and soil salt and alkali). Potential chemical reactions may occur in desert saline and alkaline soils under the influence of soil moisture, resulting in carbonate dissolution and promoting CO_2 absorption by the soil (Stone et al. 2008; Xie et al. 2009). The reduction in soil temperature (Parsonset al., 2004; Ball et al., 2009; Hamerlynck et al., 2013) and increase in soil moisture (Cuezva et al., 2011; Fa et al., 2015) can exacerbate the CO_2 absorption by the soil. By quantitatively resolving organic and inorganic contributions to the soil CO_2 flux process in saline and alkaline soil, it was proven that soil inorganic CO_2 flux plays an important role in desert ecosystems, and soil inorganic CO_2 flux at night is the main cause of carbon sequestration. In addition, it was discovered that saline and alkaline desert soils with a high pH can facilitate, in lower temperatures, the promotion of CO_2 absorption by the soil (Wang et al., 2013). Similarly, Ma et al. (2013 and 2014) carried out studies on soil CO_2 flux in the Gurbantünggüt Desert and found that CO_2 absorption by the soil may occur under the effects of inorganic processes. When soil is extremely arid, soil CO_2 flux occurs completely due to inorganic processes. In such cases, inorganic processes are controlled by soil temperature, and soil pH to some extent affects the amplitude of variation of soil CO_2 flux. At present, the main abiotic processes of soil carbon sequestration might be as follows: (1) variation in the volume of gases caused by changes in pressure and temperature governed by the ideal gas law; (2) change in solubility of CO_2 in soil–water films governed by Henry's Law; (3) pH-mediated CO_2 dissolution chemistry; and (4) surface adhesion of CO_2 onto soil minerals (Parsons et al., 2004; Xie et al., 2009; Fa et al., 2015). However, these speculated processes may not be well suited for extremely arid regions (Schlesinger et al., 2009.; Fa et al., 2016). In view of this, Fa et al. (2016) carried out an analysis on soil CO_2 flux in the Mu Us desert and pointed out that surface turbulence, air volume expansion, exudation of CO_2 dissolved in soil water, and carbonate precipitation are the primary processes causing CO_2 release from the desert. Alternatively, the downward mass flow of soil CO_2, air volume contraction, dissolution of CO_2 in soil moisture, and carbonate decomposition are also phenomena that cause CO_2 to be absorbed by desert.

The Taklimakan Desert (TD) is the world's second-largest shifting desert. The latest research indicates that the rich underground saline water in the TD has the effect of inorganic carbon-sink similar to the ocean, and its carbon storage capacity is huge. Leaching process promotes the CO_2 absorbed by the TD gradually collect into the underground saline water layer under the vast desert (Li et al., 2015). However, the contributions of the internal processes of the TD to its carbon-sink and the long-term trend of the TD carbon-sink under climate change are still unclear. In this study, through experiments of dismantling and temperature-controlled, we found that the expansion/contraction of soil air containing CO_2 caused by heat fluctuation, in combination with salts/alkali chemistry dominates the release/absorption processes of CO_2 in shifting sand. Finally, combined with historical soil temperature data and the Fifth Coupled Model Intercomparison Project (CMIP5) simulations, we reveal a stable carbon-sink property of the TD shifting sand; but as the climate changes, the carbon-sink effect will continue to decrease. This result will undoubtedly facilitate a positive feedback effect with climate change and enhance regional warming in the future. Our findings are very important for re-recognizing the status of deserts in the carbon-cycle, narrowing the gap in the missing carbon-sink and assessing the global carbon-cycle.

2 Materials and Methods

2.1 Site description

The surface of TD is mainly covered by a wide range of highly homogeneous shifting sand. In addition, the environmental conditions at the three monitoring sites from north to south are basically consistent, especially as regards soil temperature (Figure 1). Therefore, Tazhong located in the hinterland of the desert can be considered as the most representative research area in the TD. This study was conducted in the Tazhong shifting sand land (38° 58′ N, 83° 39′ E, 1099 m above sea level). The entire region has a continental warm temperate arid desert climate. The annual mean precipitation is 25.9 mm, and the intra-annual distribution is exceedingly non-uniform, with precipitation concentrated in May–August. The annual potential evaporation is 3812.3 mm. The region has four distinct seasons and a high diurnal temperature range. The mean annual temperature is 12.1 °C, with maximum temperatures of 40.0–46.0 °C and minimum temperatures of –20.0 to –32.6 °C (Yang et al., 2017; Zhou et al., 2019). Poor environmental conditions have resulted in a severe deficiency in animal- and plant-based resources in this region. The total area of shifting sand in the TD is approximately 2.364×10^{11} m^2, covering approximately 70% of the TD (http://westdc.westgis.ac.cn). The shifting sand consists of silt and clay (1.5%), fine sand and very fine sand (88.8%) grains, and medium sand (9.7%) grains. The average particle size of the sand is 0.083–0.129 mm, with a standard deviation between 0.03 and 0.98 mm. Surface sand in this region is finer than that in other deserts (Huo et al., 2011; Yang et al., 2016a). Table 1 displays the physiochemical traits of the shifting sand. The region experiences prevailing easterly winds throughout the year, with an annual mean of 11 days with gale-force weather, more than 157 days of floating dust and blowing sand, and an annual mean of 16 days with sandstorms (Yang et al., 2016b). The aeolian landforms mainly consist of linear, high, and composite longitudinal dunes and inter-dune corridors. The dunes are oriented NNE—SSW or NE—SW, and their relative height is 40–50 m.

2.2 Disassembly experiment

To facilitate an analysis of the contributions of various components of TD shifting sand to CO_2 exchange and to account for the fact that shifting sand has a simple structure, we hypothesize that total CO_2 flux in shifting sand (R_s) is the sum of the contributions from sand (R_{sand}), moisture ($R_{moisture}$), salt/alkali ($R_{salt/alkali}$) and microbes ($R_{microbe}$) (Equation 1). The four processes involved in the CO_2 flux of the shifting sand fully agree with the current consensus regarding the CO_2 flux of shifting sand (Parsons et al., 2004; Fa et al., 2014 and 2016). Complex interactions between the various components and changes in carbon storage capacity of each process will be considered in future studies.

$$R_s = R_{sand} + R_{moisture} + R_{salt/alkali} + R_{microbe} \quad (1)$$

We collected topsoil (0–10 cm) from the study site, submitting samples to gradual dealkalization/desalination followed by autoclaving and subsequent drying. We obtained a mean gravimetric soil water content of 0.0013 kg kg^{-1} within 10 cm of the surface layer of the shifting sand through soil drying. Using this value of soil water content, moisture was restored in

Samples 2 and 3 after drying to replicate field conditions. Table 2 shows detailed treatment methods for each soil sample.

As shown in Figure 2 Left, the four samples that were allowed to stand and equilibrate were placed in plastic trays (diameter 40 cm, height 18 cm). One day before CO_2 flux measurements were taken, the four samples and their plastic trays were buried in the shifting sand, 20 m from the 3 m high land-atmosphere interaction observation tower. Levels of shifting sand inside and outside the tray were kept the same. Four cylindrical soil collars (cross-sectional area of 371.8 cm^2 and height of 10 cm) were embedded in the four samples, up to a depth of 8 cm. From October 10, 2017, to October 18, 2017, an automatic CO_2 flux measurement system (Model LI-8100A fitted with a LI-8150 multiplexer, LI-COR, Nebraska, USA), equipped with four LI-8100-104 long-term monitoring chambers, was used for whole-day continuous and synchronous monitoring of daily CO_2 flux dynamics in the four samples. Because CO_2 fluxes are weak in deserts, we calibrated the analyser before obtaining the measurements to ensure precision and appropriately extended the duration of the entire measurement process. Further details of the instrument settings on field measurements can be found in Yang et al. (2017). During the measurement, the LI-8100A seal ring was cleaned 3 times a day to ensure the airtightness of chamber. In addition, to increase confidence in the application of the LI-8100A instrument to a desert environment, we conducted evaluation experiments in the study area. The bottoms of the soil collars were completely sealed with plastic film and buried in the shifting sand. The plastic film blocked CO_2 exchange between shifting sand and atmosphere. The CO_2 flux of the four chambers did not change with changes in the external conditions, and values were all concentrated near zero with an accuracy of ±0.02 $umol \cdot m^{-2} \cdot s^{-1}$ (Figure omitted). Therefore, the shifting sand CO_2 flux obtained by the LI-8100A in this study is reliable and accurate. Finally, using step-by-step dismantling, we obtained CO_2 flux data for various components in the TD shifting sand.

2.3 Temperature-controlled experiment

This temperature-controlled experiment was conducted in the basement of the Taklimakan Desert meteorological field experiment station to avoid complex and uncontrollable environmental conditions in the field (Figure 2 Right). During the experimental period, the air temperature in the basement was maintained at approximately 10 °C; the air temperature variation during the experiment did not exceed 0.79 °C. The mean relative air humidity was 18.32%, and the variation did not exceed 2.9%. The carbon dioxide concentration was maintained at approximately 405.8 ppm.

Based on the treatment method for Sample 4, sand samples were packed into two plastic boxes (length 60 cm, width 45 cm, and height 20 cm). Soil collars were embedded in the boxes. A heating wire was evenly placed with a spacing of 2 cm on the surface of the sand in one of the plastic boxes. The temperature of the sand was controlled by adjusting the voltage of the heating wire (Figure 2 Right). The second box was used as a control and was not heated. From November 21–25, 2017, an automatic CO_2 flux measurement system was used for synchronous and continuous monitoring of CO_2 flux in the sand after these two heating treatments. Device settings were identical to those used in the field monitoring experiment. Soil temperature sensors (Model 109, Campbell, USA) were installed at depths of 0 cm and 10 cm in the sand in the two plastic boxes to obtain soil temperature at the corresponding depths (T_{0cm} and T_{10cm}).

2.4 Statistical analysis

SPSS 16.0 was used for the differential analysis of CO_2 fluxes corresponding to the different treatments. SigmaPlot 14.0 was used for correlation and regression analyses of the CO_2 flux, soil temperature difference between 0 cm and 10 cm ($T_{0–10cm}$, °C), and rate of soil temperature change at 10 cm ($\Delta T_{10cm}/\Delta t$, °C•min^{-1}; soil temperature difference at 10 cm every minutes between two consecutive CO_2 flux measurements). Four common non-linear equations were used to analyse the synergistic effects of $T_{0–10cm}$ and $\Delta T_{10cm}/\Delta t$ on CO_2 flux:

$$R = a + b\ T_{0–10cm} + c\ (\Delta T_{10cm}/\Delta t) \quad (2)$$

$$R = a + b\ T_{0–10cm} + c\ (\Delta T_{10cm}/\Delta t) + d\ T_{0–10cm}\ (\Delta T_{10cm}/\Delta t) \quad (3)$$

$$R = a + b\ T_{0–10cm} + c\ (\Delta T_{10cm}/\Delta t) + d\ (T_{0–10cm})^2 + e\ (\Delta T_{10cm}/\Delta t)^2 \quad (4)$$

$$R = a\ T_{0–10cm}^{\ b}\ (\Delta T_{10cm}/\Delta t)^c \quad (5)$$

where R is CO_2 flux (such as R_{sand} or R_s), and a, b, c, d, and e are fitting parameters.

2.5 Estimation of historical CO_2 exchange in TD shifting sand

Based on the regression equations above, we selected the best fitting equation for R_{sand} or R_s, and in combination with the soil temperature observations in the study area at 0 cm and 10 cm every hour between 2004 and 2017, we estimated the corresponding CO_2 flux. By gradual accumulation and area expansion, the total amount of CO_2 exchange in TD shifting sand was obtained annually 2004 to 2017.

2.6 Future trends in total CO_2 exchange in TD shifting sand

We would like to use the relationship between soil temperature ($T_{0–10cm}$ and$\Delta T_{10cm}/\Delta t$) and CO_2 flux in combination with average soil temperature prediction data from multiple models in CMIP5 to expand the timescale across which the relationship is assessed and reflect future CO_2 exchange in TD shifting sand. However, several problems must first be overcome. Eight models were selected from CMIP5 that cover simulated data for monthly mean soil temperatures from 2006 to 2100. The simulated surface temperatures data were separately verified using monthly mean surface temperature data measured in 2006–2017 in the study area. The three models with the best simulation results were identified. These three models have different soil depth levels and do not directly provide soil temperature at a 10 cm depth. Using the regression relationship between the observed monthly means of soil temperature at depths of 0 cm and 10 cm in the study area from 2006 to 2017, combined with the average surface temperatures of the selected three models, soil temperature at 10 cm depth was calculated. The monthly average $T_{0–10cm}$ was obtained from 2017 to 2100. $\Delta T_{10cm}/\Delta t$ does not have the original physical meaning on the monthly time scale, so the previously established regression relationship between CO_2 flux, $T_{0–10cm}$, and $\Delta T_{10cm}/\Delta t$ cannot be directly applied. Using historical soil temperature data and monthly values of cumulative CO_2 exchange obtained in the previous section, we re-established a relationship between cumulative monthly CO_2 flux and monthly average $T_{0–10cm}$. There was a good linear regression relationship between T_{0-10cm} and the CO_2 flux of the Taklimakan Desert shifting sand at the monthly scale:

$$R_s = 13641 \times T_{0-10cm} - 18814 \qquad R^2=0.928 \quad (6)$$

where R_s (umol m^{-2} month^{-1}) is the CO_2 flux at the monthly scale and T_{0-10cm} is the soil temperature difference between the 0 and 10 cm depth at the monthly scale. Finally, the total amount of CO_2 exchange per year in TD shifting sand from 2018 to 2100 was obtained under the RCP4.5 and RCP8.5 scenarios.

3 Results

3.1 Contribution of component processes to total CO_2 flux

By stepwise subtraction, we obtained the contribution of the CO_2 fluxes of various components in the TD shifting sand, which were shown in Figure 3. Comparing demonstrate that contributions of sand and salts/alkalis to the total CO_2 flux in the Tazhong shifting sand are extremely significant, dominating the release and absorption, respectively, of CO_2 in shifting sand. For sand, its diurnal pattern shows unimodal curves with higher intensity than that of the total CO_2 flux in shifting sand. During the day, sand promotes CO_2 release into the atmosphere, which reaches a peak (0.143 $\mu mol\cdot m^{-2}$) at 15:15 h (Beijing time, used hereafter). During night, sand promotes stable CO_2 absorption from the atmosphere, with a mean rate of –0.026 $\mu mol\cdot m^{-2}$. This study is the first time that this unconventional phenomenon has been documented in CO_2 flux studies over the TD region. Due to the lack of a satisfactory explanation for this stimulating effect of sand, we designed subsequent temperature-controlled experiments and provided explanations for the mechanisms affecting the diurnal pattern of this sand CO_2 flux. The contribution of moisture to the total CO_2 flux is very limited, with a rate ranging from –0.051 to 0.011 $\mu mol\cdot m^{-2}\cdot s^{-1}$. During the entire day, moisture promotes the release of CO_2 to the atmosphere between 15:45 and 19:15 h, and promotes atmospheric CO_2 absorption for the remaining time. As moisture provides a relatively small contribution to the CO_2 flux, subsequent experiments focused only on the effects of soil temperature over the CO_2 flux. During the day, salts/alkalis strongly promote atmospheric CO_2 absorption, reaching a peak (–0.106 $\mu mol\cdot m^{-2}$) at 14:15 h. Whereas in the night, salts/alkalis promote stable CO_2 release in to the atmosphere. Microbes consistently cause a small amount of CO_2 released into the atmosphere; and these effects being more pronounced during the day than night. The total CO_2 flux is significantly lower in shifting sand, which contains a superimposition of various components, than in other ecosystems, with a negative flux occasionally present during the night (Lou and Zhou, 2006; Yang et al., 2017). The daily mean rate was 28.7×10^{-3} $\mu mol\cdot m^{-2}\cdot s^{-1}$, and the daily variation ranged from –0.026 to 0.101 $\mu mol\cdot m^{-2}\cdot s^{-1}$.

3. 2 Driving mechanisms of CO_2 release/absorption in sand

From the temperature-controlled experiments, we can see that the sand temperatures without temperature-control regulation were relatively stable and temperature fluctuations in various layers during the entire observation period did not exceed 1 °C. The corresponding CO_2 flux is generally stable at approximately zero. In contrast, under temperature-controlled regulation, sand exhibits a significant CO_2 absorption/release, the changing rhythm of which is generally consistent with soil temperature variations (Figure 4). In the red region, the CO_2 flux increases when soil temperatures increase. When the soil temperature rapidly decreases (as shown in the blue region), the CO_2 flux changes from initially positive to negative values. Therefore, the soil temperature is the most critical driver of CO_2 exchange in sand (Fang and Moncrieff, 2001; Sánchez et al., 2003; Rodeghiero and Cescatti, 2005). However, once soil temperatures become relatively stable, the CO_2 flux intensity begins to exhibit a decreasing trend and gradually approaches zero.

Based on the above information and considering that a CO_2 flux is the overall performance of the soil surface layer (Lou and Zhou, 2006), we assert that a soil temperature difference between depths of 0 and 10 cm ($T_{0–10cm}$) and the rate of soil temperature change at a depth of 10 cm ($\Delta T_{10cm}/\Delta t$) are the two main factors driving CO_2 exchange in sand (R_{sand}). $T_{0–10cm}$ represents the flow and intensity of soil heat, and $\Delta T_{10cm}/\Delta t$ represents heat absorption/release by the soil (Parsons et al., 2004; Ball et al., 2009). Compared to soil temperature, $T_{0–10cm}$ and $\Delta T_{10cm}/\Delta t$ show higher consistency with R_{sand}, presenting significant linear and quadratic regression relationships, respectively (Figure 5). The aforementioned consistency can be enhanced, which is more evident after the soil temperature becomes stable. Therefore, we speculated that the expansion/contraction of soil air containing CO_2 by heat transmission causes sand to experience a CO_2 release/absorption phenomenon. The intense increase/decrease in soil temperature promotes the expansion/contraction of soil air and the intense release/absorption of CO_2. The loose porous structure of sand allows for the expansion/contraction of soil air during intense temperature changes. In addition, an analysis of synergistic effects shows that Equation 4 can well explain the comprehensive response of R_{sand} to variation in $T_{0–10cm}$ and $\Delta T_{10cm}/\Delta t$ (Table 3). Through Equation 4 and historical observation data on soil temperature, the estimated values of R_{sand} show good agreement with the observed values (Figure 6).

3.3 Effect of $T_{0–10cm}$ and $\Delta T_{10cm}/\Delta t$ on R_s

Through disassembly experiments, we found that soil temperature is the key factor to control the contribution of various shifting sand components to the total CO_2 flux in the shifting sand. Therefore, we selected the monitoring data of the shifting sand CO_2 flux in the study region and corresponding soil temperatures of two layers (T_{0cm} and T_{10cm}) on January 17–31, 2013, October 17–23, 2013, May 4–7, 2015, and July 16–23, 2019, for analysis (Figure 7). $T_{0–10cm}$ and $\Delta T_{10cm}/\Delta t$ show good consistency with R_s with significant linear regression relationships (R^2=0.756 and 0.501, respectively; $P < 0.001$). Thus, we analysed the synergistic effects of $T_{0–10cm}$ and $\Delta T_{10cm}/\Delta t$ on R_s (Table 3). Except for a failed fitting analysis when using Equation 5, the other three equations explain the comprehensive responses of R_s to variation in $T_{0–10cm}$ and $\Delta T_{10cm}/\Delta t$ ($R^2 > 0.756$) well and to a highly significant level ($P < 0.001$). This result indicates that the synergistic effects of $T_{0–10cm}$ and $\Delta T_{10cm}/\Delta t$ are the major factors driving the CO_2 flux in the sand, and the main factors influencing the total CO_2 flux in shifting sand. In addition to sand, other components also respond well to $T_{0–10cm}$ and $\Delta T_{10cm}/\Delta t$. Using Equation 4 and corresponding observational data on soil temperature in different periods, the estimated values of R_s show good agreement with the observed values (Figure 8).

3.4 Response of TD shifting sand carbon-sink to future climatic change

Figure 9a shows that the mutual counteraction of the effect of thermal expansion of soil air containing CO_2 and the effect of remaining components (salt/alkali + moisture + microbes) caused the TD shifting sand to exhibit a clear and stable carbon-sink effect, with an annual carbon-sink rate of 1.60×10^6 $t \cdot a^{-1}$. Between 2004 and 2017, both processes increased over time. However, the increase rate of CO_2 released was higher than that of CO_2 absorption, which eventually caused an annually weakening trend in the carbon-sink effect of the TD shifting sand. According to the relationship between T_{0-10cm} and the carbon-sink effect of TD shifting sand, increasing T_{0-10cm} (Figure 9c) in the future will more strongly stimulate the thermal expansion of soil air, pumping more CO_2 into the atmosphere, which will eventually lead to the gradual weakening of the carbon-sink property of TD shifting sand. As shown in Figure 9b, the carbon-sink effect of TD shifting sand will decrease at a rate of 0.42% and 1.42% per year under RCP4.5 and RCP8.5, respectively. Notably, the entire shifting sand surface in the TD will reach a CO_2 absorption/release neutral state in approximately 2090 under RCP8.5, and ~0.475 × 10^6 t of CO_2 would be released annually until 2100. The weakening of carbon-sink processes is more pronounced under the RCP8.5 scenario.

4 Discussion

Soil temperature and moisture are the two most important factors affecting soil CO_2 exchange (Wildung et al., 1975; Tang and Baldocchi, 2005; Sierra, 2012). However, due to the prominent role of abiotic processes in CO_2 exchange in desert ecosystems, the response of desert ecosystems to these two factors is different from other types of ecosystems. Through field observations, we found that the expansion/contraction of soil air containing CO_2 is caused by soil temperature fluctuations, presenting an unexpected contribution to total CO_2 exchange. Salt/alkali strongly promotes shifting sand to absorb atmospheric CO_2 during the day and release CO_2 at night. The combined effects of this process and the expansion/contraction of soil air dominate the absorption/release of CO_2 in shifting sand. However, the contribution of salt/alkali in the TD is opposite to that in Gurbantunggut Desert (Ma et al., 2013 and 2014; Xie et al., 2009; Wang et al., 2013). This peculiarity warrants further research and analysis. In the extremely dry TD, minor fluctuations in soil moisture are not sufficient to overcome the limiting effects of drought on CO_2 exchange, resulting in moisture contributing extremely limitedly to CO_2 exchange in shifting sand. This scenario provides a new understanding of the role of moisture in the desert carbon-cycle. The weak contribution of microbes to the total CO_2 flux indicates that microbial activity in the TD is very weak. However, this information also shows that the desert is not as lifeless as it seems.

The superimposition of several processes causes TD shifting sand to exhibit an incredible carbon-sink effect, with an annual average carbon-sink rate of 1.60×10^6 $t\cdot a^{-1}$ during 2004–2017. Leaching process promotes the CO_2 absorbed by the TD gradually collect into the underground saline water layer under the vast desert (Ma et al., 2014; Li et al., 2015). The TD shifting sand only accounts for ~0.747% of the global desert area. If all global shifting deserts are considered, and the carbon-sink rate obtained in this study represents an average state, then the global shifting desert maybe absorb ~2.125×10^8 t of CO_2 per year. It can help to reduce the missing carbon-sink in global carbon-cycle.

Global warming will accelerate the decomposition of organic carbon, releasing large amounts of CO_2 into the atmosphere (Bond-Lamberty and Thomson, 2010; Giardina et al., 2014). However, for desert ecosystems with extremely low organic carbon reserves, increases in $T_{0\text{-}10cm}$ due to climate change will strongly stimulate the future thermal expansion of soil air, releasing more CO_2 from sand into the atmosphere. This process will eventually lead to a gradual weakening of the carbon-sink in TD shifting sand. Under RCP4.5 and RCP8.5, the carbon-sink rate of CO_2 in TD shifting sand will decrease by 0.42% and 1.40% per year, respectively. Under RCP8.5, ~0.475×10^6 t of CO_2 would be released annually until 2100. This process would facilitate a positive feedback effect on the climate change and cause enhanced regional warming (Rustad et al., 2000; Friedlingstein et al., 2003; Huang et al., 2016). Desert ecosystems, which have not been valued for a long time, have always playing an important role of carbon-sink in obscurity. However, a gradual reduction in the deserts carbon-sink will put forward more urgent requirements for the formulation of climate change countermeasures.

5 Conclusions

Through experiments of dismantling and temperature-controlle, our study quantifies the exact magnitude and process of the CO_2 fluxes for each component of the shifting sand in the TD, especially the expansion/contraction of soil air containing CO_2 caused by heat fluctuation, which is easily neglected, and the exaggerated effect of soil moisture on CO_2 flux in a desert environment. Furthermore, the absorption effect of CO_2 by saline/alkali in the desert was confirmed. Finally, we found that the Taklimakan Desert shifting sand currently acts as a stable carbon-sink that had an annual CO_2 uptake of 1.60×10^6 $t \cdot a^{-1}$ during 2004-2017. If all global shifting deserts are considered, the status of desert ecosystems in the global carbon-cycle cannot be simply ignored. It can help to reduce the missing carbon-sink in global carbon-cycle. However, CMIP5 simulations indicate that the contribution of the TD shifting sand carbon-sink will decrease in the future through over-stimulation of the unnoticed temperature driven process of the soil air expansion to CO_2 release processes.

Acknowledgments

This work was jointly supported by the second Tibetan Plateau Scientific Expedition and Research Program (STEP; 2019QZKK0602), the National Natural Science Foundation of China (41521004, 41975010 and 41175140) and the China University Research Talents Recruitment Program (111 project, NO. B13045). The authors would also like to thank the Taklimakan Desert Meteorology Field Experiment Station of CMA for providing observation instruments and data. The data of CMIP5 model simulations can be obtained from https://esgf-node.llnl.gov/search/cmip5. The main observation data involved in the manuscript have been uploaded together with the manuscript as supplements for the review purpose. If the manuscript is published successfully, we will put all the experimental data in the designated location according to the data policy, and provide the accurate storage location for the readers to download.

References

Post, W. M., Emanuel, W. R., Zinke, P. J., & Stangenberger, A. G. (1982). Soil carbon pools & world life zones. *Nature*, 298(5870), 156-159.

Jobbagy, E. E. G., & Jackson, R. B. (2000). The vertical distribution of soil organic carbon and its relation to climate and vegetation. *Ecological Applications*, 10(2), 423-436.

Batjes, N. H. (1996). Total carbon and nitrogen in the soils of world. *European Journal of Soil Science*, 47(2), 151-163.

Raich, J. W., & Potter, C. S. (1995). Global patterns of carbon dioxide emissions from soils. *Global Biogeochem Cycles*, 9(1), 23-36.

Singh J. S., & Gupta, S. R. (1977). Plant decomposition and soil respiration in terrestrial ecosystems. *Botanical Review*, 43(4), 449-528.

Schlesinger, W. H., & Andrews, J. A. (2000). Soil respiration and the global carbon cycle. *Biogeochemistry*, 48(1), 7-20.

Lou, Y. Q., & Zhou, X. H. (2006). Soil respiration and the environment. San Diego, pp. 1-89, Academic Press/Elsevier.

Houghton, R. A., Davidson, E. A., & G. Woodwell, M. (1998). Missing sinks, feedbacks, and understanding the role of terrestrial ecosystems in the global carbon balance. *Global Biogeochem Cycles*, 12(1), 25-34.

Rustad, L. E., Huntington, T. G., & Boone, R. D. (2000). Controls on soil respiration: implications for climate change. *Biogeochemistry*, 48(1), 1-6.

Friedlingstein, P., Bopp, L., Ciais, P., Dufresne, J. L., Fairhead, L., LeTreut, H., Monfray, P. , & Orr, J. (2001). Positive feedback between future climate change and the carbon cycle. *Geophysical Research Letters*, 28(8), 1543-1546.

Han, Q. F., Luo, G. P., Li, C. F., & Li, S. B. (2018). Response of carbon dynamics to climate change varied among different vegetation types in Central Asia. *Sustainability*, 10, 3288, doi: 10.3390/su 10093288.

Burkins, M. B., Virginia, R. A., & Wall, D. H. (2001). Organic carbon cycling in Taylor Valley, Antarctica: quantifying soil reservoirs and soil respiration. *Global Change Biology*, 7(1), 113-125.

Barrett, J. E., Virginia, R. A., Parsons, A. N., & Wall, D. H. (2006). Soil carbon turnover in the McMurdo Dry Valleys, Antarctica. *Soil Biology & Biochemistry*, 38(10), 3065-3082.

Hopkins, D. W., Sparrow, A. D., Elberling, B., Gregorich, E. G., Novis, P. M., Greenfield, L. G., & Tilston, E. L. (2006). Carbon, nitrogen and temperature controls on microbial activity in soils from an Antarctic dry valley. *Soil Biology & Biochemistry*, 38(10), 3130-3140.

Li, C. F., Han, Q. F., Luo, G. P., Zhao, C. Y., Li, S. B., Wang, Y. G., & Yu, D. S. (2018). Effects of cropland conversion and climate change on agrosystem carbon balance of China's dryland: a typical watershed study. *Sustainability*, 10, 4508, doi: 10.3390/su 10124508.

Parsons, A. N., Barrett, J. E., Wall, D. H., & Virginia, R. A. (2004). Soil carbon dioxide flux in Antarctic dry valley ecosystems. *Ecosystems*, 7(3), 286-295.

Shanhun, F. L., Almond, P. C., Clough, T. J., & C. Smith, M. S. (2012). Abiotic processes dominate CO_2 fluxes in Antarctic soils. *Soil Biology & Biochemistry*, 53, 99-111.

Barrett, J. E., Virginia, R. A., Wall, D. H., & Adams, B. J. (2008). Decline in a dominant invertebrate species contributes to altered carbon cycling in a low-diversity soil ecosystem. *Global Change Biology*, 14(8), 1734-1744.

Stone, R. (2008). Have desert researchers discovered a hidden loop in the carbon cycle? *Science*, 320(5882), 1409-1410.

Xie, J. X., Li, Y., Zhai, C. X., Li, C. H., & Lan, Z. D. (2009). CO_2 absorption by alkaline soils and its implication to the global carbon cycle. *Environmental Geology*, 56(5), 953-961.

Ball, B. A., Virginia, R. A., Barrett, J. E., Parsons, A. N., & Wall, D. H. (2009). Interactions between physical and biotic factors influence CO_2 flux in Antarctic dry valley soils. *Soil Biology & Biochemistry*, 41(7), 1510-1517.

Hamerlynck, E. P., Scott, R. L., Sánchez-Cañete, E. P., & Barron-Gafford, G. A. (2013). Nocturnal soil CO_2 uptake and its relationship to subsurface soil and ecosystem carbon fluxes in a Chihuahuan Desert shrubland. *Journal of Geophysical Research-Biogeosciences*, 118(4), 1593-

1603.

Cuezva, S., Fernandez-Cortes, A., Benavente, D., Serrano-Ortiz, P., Kowalski, A. S., & Sanchez-Moral, S. (2011). Short-term CO_2(g) exchange between a shallow karstic cavity and the external atmosphere during summer: Role of the surface soil layer. *Atmospheric Environment*, 45(7), 1418-1427.

Fa, K. Y., Liu, J. B., Zhang, Y. Q., Wu, B., Qin, S. G., Feng, W., & Lai, Z. R. (2014). CO_2 absorption of sandy soil induced by rainfall pulses in a desert ecosystem. *Hydrological Processes*, 29(8), 2043-2051.

Wang, Z. Y., Xie, J. B., Wang, Y. G., & Li, Y. (2013). Soil inorganic CO_2 flux in relation to soil pH and electric conductivity in saline/alkaline soils. *Chinese Journal of Ecology*, 32(10), 2552-2558. (in Chinese)

Ma, J., Wang, Z. Y., Stevenson, B. A., Zheng, X. J., & Li, Y. (2013). An inorganic CO_2 diffusion and dissolution process explains negative CO_2 fluxes in saline/alkaline soils. *Scientific Reports*, 3(6), doi: 10. 1038/srep02025.

Ma, J., Liu, R., Tang, L. S., Lan, Z. D., & Li, Y. (2014). A downward CO_2 flux seems to have nowhere to go. *Biogeosciences*, 11(22), 6251-6262.

Schlesinger, W. H., Belnap, J., & Marion, G. (2009). On carbon sequestration in desert ecosystems. Global Change Biology, 15(6), 1488-1490.

Fa, K. Y., Zhang, Y. Q., Wu, B., Qin, S. G., Liu, Z., & She, W. W. (2016). Patterns and possible mechanisms of soil CO_2 uptake in sandy soil. *Science of the Total Environment*, 544, 587-594.

Li, Y,, Wang, Y. G., Houghton, R. A., & Tang, L. S. (2015). Hidden carbon sink beneath desert. *Geophysical Research Letters*, 42(14), 5880-5887.

Yang, F., Ali, M., Zheng, X. Q., He, Q., Yang, X. H., Huo, W., Liang, F. C., & Wang, S. M. (2017). Diurnal dynamics of soil respiration and the influencing factors for three land-cover types in the hinterland of the Taklimakan Desert, China. *Journal of Arid Land*, 9(4), 568-579.

Zhou, C. L., Ali, M., Yang, F., Huo, W., Wang, M. Z., Pan, H. L., He, Q., Jin, L. L., & Yang, X. H. (2019). Dust uplift potential in the Taklimakan Desert: an analysis based on different wind speed measurement intervals. *Theoretical and Applied Climatology*, 137(1-2), 1449-1456.

Wang, Y. M., Wang, J. H., & Yan, C. Z. (2005). Cold and Arid Regions Science Data Center at Lanzhou. doi:10.3972/westdc.006.2013.db.

Huo, W., He, Q., Yang, X. H., Liu, X. C., Ding, G. F., & Cheng, Y. J. (2011). The research on grain size characteristic of desert in north of China. *Research of Soil and Water Conservation*, 18(6), 6-11. (in Chinese).

Yang, X. H., Yang, F., Liu, X. C., Huo, W., Ali, M., & Zhang, Q. Y. (2016a). Comparison of horizontal dust fluxes simulated with two dust emission schemes based on field experiments in Xinjiang, China. *Theoretical and Applied Climatology*, 126(1-2), 223-231.

Gu, F. X., Wen, Q. K., Pan, B. R., & Yang, Y. S. (2000). A preliminary study on soil micooriganisms of artificial vegetation in the center of Taklimakan Desert. *Chinese Biodiversity*, 8(3), 297-303. (in Chinese).

Yang, X. H., Shen, S. H., Yang, F., He, Q., Ali, M., Huo, W., & Liu, X. C. (2016b). Spatial and temporal variations of blowing dust events in the Taklimakan Desert. *Theoretical and Applied Climatology*, 125(3-4), 669-677.

Fang, C., & Moncrieff, J. B. (2001). The dependence of soil CO_2 efflux on temperature. *Soil Biology & Biochemistry*, 33(2), 155-165.

Sánchez, M. L., Ozores, M. I., López, M. J., Colle, R., Torre, B. De, M. García, A., Pérez, I. (2003). Soil CO_2 fluxes beneath barley on the central Spanish plateau. *Agricultural and Forest Meteorology*, 118(1-2), 85-95.

Rodeghiero, M., & Cescatti, A. (2005). Main determinants of forest soil respiration along an elevation/temperature gradient in the Italian Alps. *Global Change Biology*, 11(7), 1024-1041.

Wildung, R. E., Garland, T. R., & Buschbom, R. L. (1975). The interdependent effects of soil temperature and water content on soil respiration rate and plant root decomposition in arid grassland soils. *Soil Biology & Biochemistry*, 7(6), 373-378.

Tang, J. W., & Baldocchi, D. D. (2005). Spatial–temporal variation in soil respiration in an oak–grass savanna ecosystem in California and its partitioning into autotrophic and heterotrophic components. *Biogeochemistry*, 73(1), 183-207.

Sierra, C. A. (2012). Temperature sensitivity of organic matter decomposition in the Arrhenius equation: some theoretical considerations. *Biogeochemistry*, 108(1-3), 1-15.

Bond-Lamberty, B., & Thomson, A. (2010). Temperature-associated increases in the global soil respiration record. *Nature*, 464(7288), 579-582.

Giardina, C. P., Litton, C. M., Crow, S. E., & Asner, G. P. (2014). Warming-related increases in soil CO_2 efflux are explained by increased below-ground carbon flux. *Nature Climate Change*, 4(9), 822-827.

Huang, J. P., Yu, H. P., Guan, X. D., Wang, G. Y., & Guo, R. X. (2016). Accelerated dryland expansion under climate change. Nature Climate Change, 6(2), 166-171.

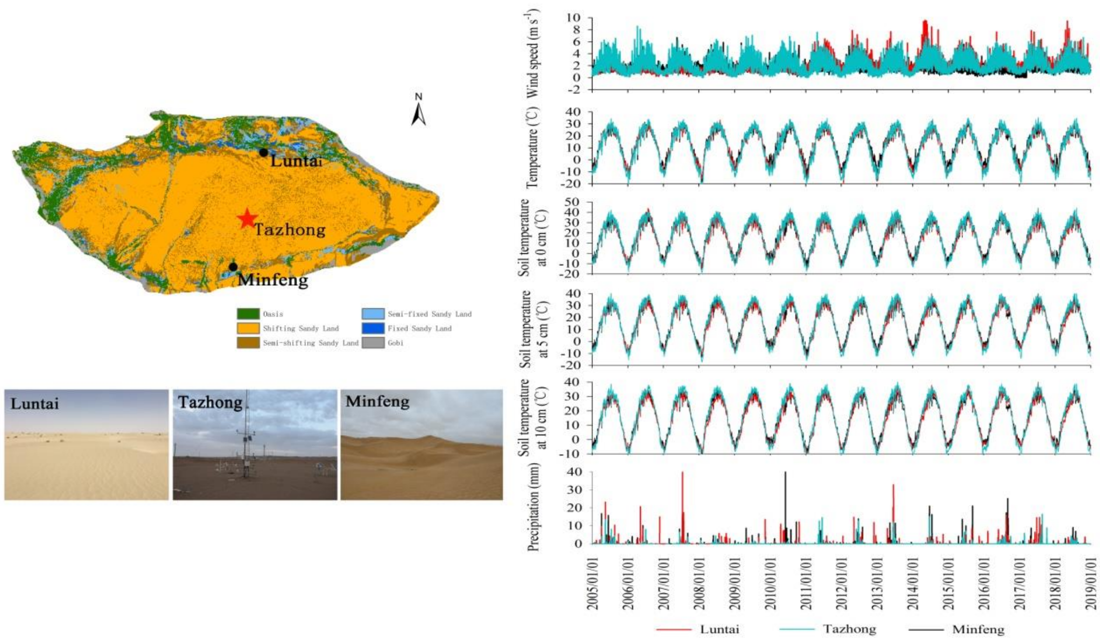

Figure 1. Left: Distribution of land cover types in the TD and the geographical location of Tazhong (red star). Landscape photographs of different locations in the TD show that the surface is mainly covered by a wide range of highly homogeneous shifting sand. Right: Comparison of the environmental conditions of the three monitoring points (Luntai, Tazhong, and Minfeng) from north to south of the TD.

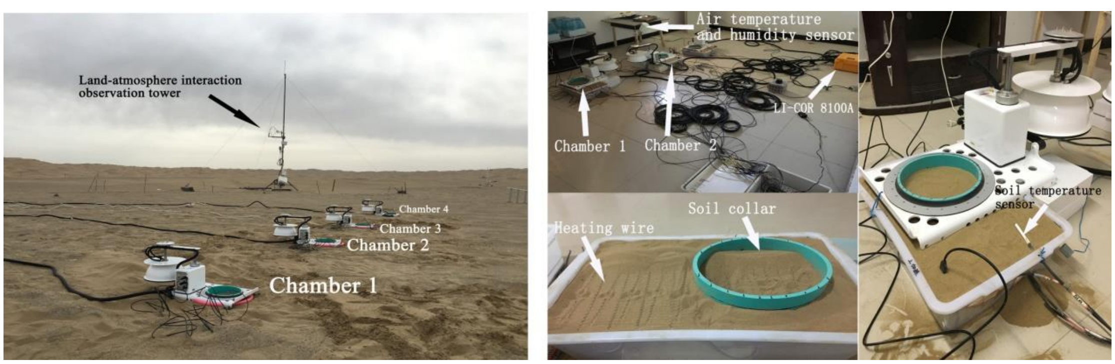

Figure 2. Layout of the CO_2 exchange experiment. Left: Field monitoring of the contributions of various shifting sand components to the total CO_2 flux. Chambers 1–4 correspond to Samples 1–4, respectively. The land-atmosphere interaction observation tower provided the historical observation data of soil temperature for this study. Right: Temperature-controlled experiment setup for CO_2 flux in sand. Heating wires were placed with a spacing of 2 cm on the surface of the sand in one of the plastic boxes. Soil collars were embedded in the sand. Soil temperature sensors were installed in the sand at depths of 0 cm and 10 cm.

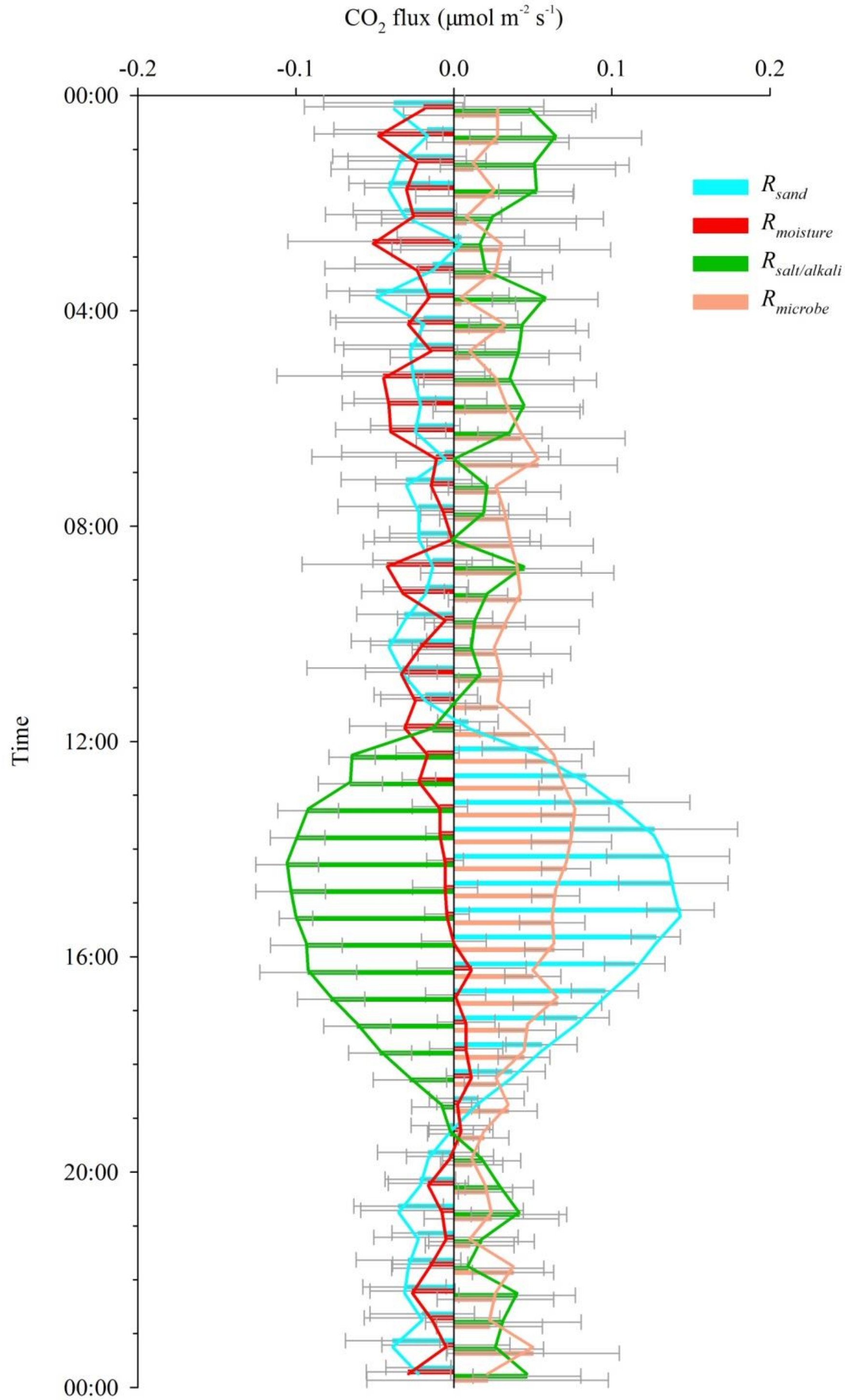

Figure 3. The contribution of different components of shifting sand to the diurnal dynamic of the total CO_2 flux of the TD shifting sand was disassembled. The diurnal contributions of CO_2 flux of each shifting sand component is expressed as R_{sand}, $R_{moisture}$, $R_{salt/alkali}$, and $R_{microbe}$, respectively. Error bars represent standard deviations.

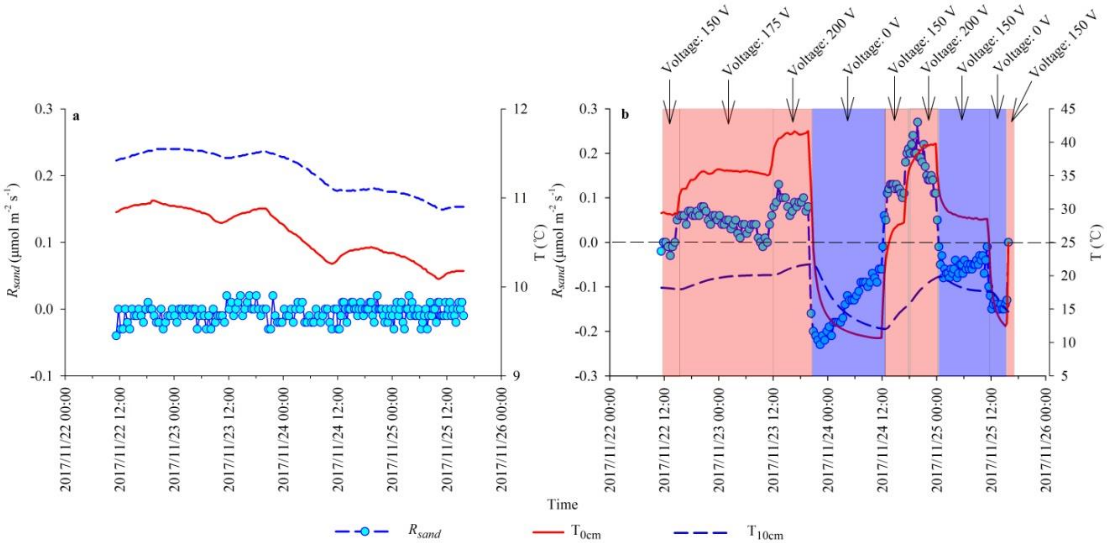

Figure 4. Relationship between R_{sand} and soil temperatures at 0 and 10 cm depths (T_{0cm} and T_{10cm}, respectively) in a temperature-controlled experiment using a voltage adjustment. a, Soil temperature not regulated. b, Soil temperature regulated. Black vertical lines separate regions of different voltages. Red regions correspond to voltage increases in comparison with the voltage in the preceding region and subsequent increases in soil temperature. Blue regions correspond to voltage decreases in comparison to the voltage of the preceding region and subsequent decreases in soil temperature.

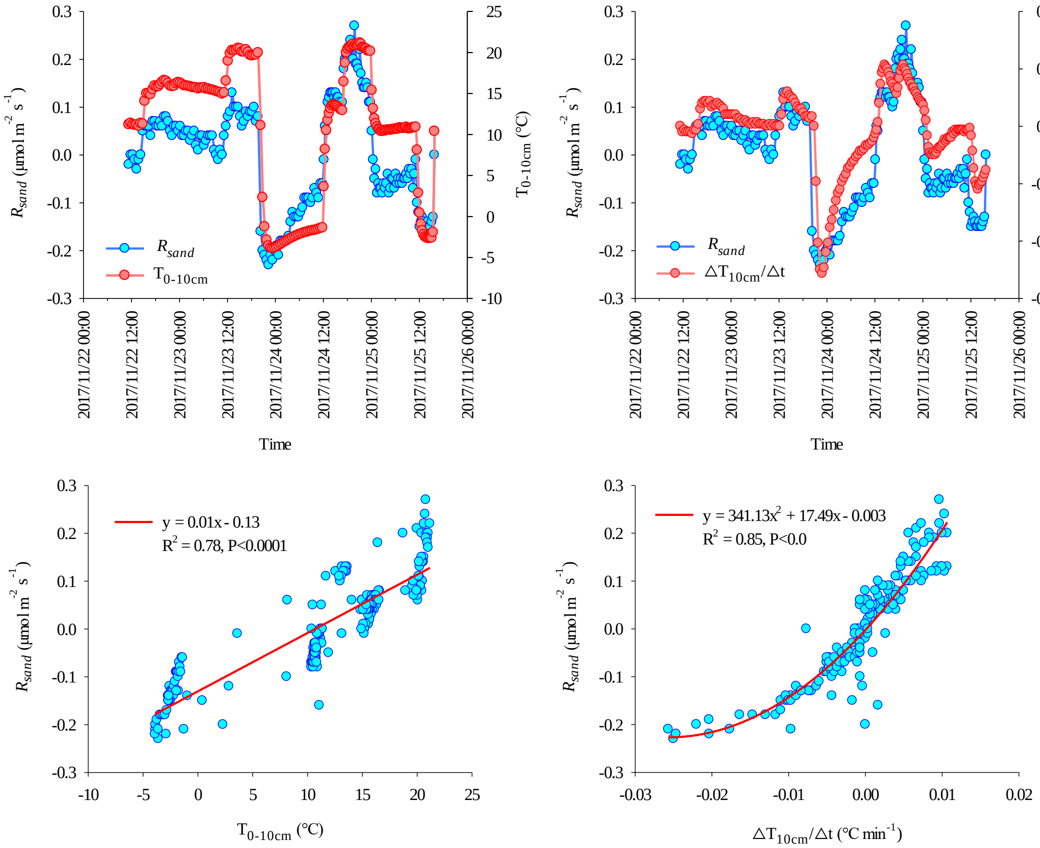

Figure 5. Relationships between $T_{0\text{–}10cm}$, $\Delta T_{10cm}/\Delta t$, and R_{sand} in temperature-controlled experiments. Left: relationship between R_{sand} and $T_{0\text{–}10cm}$; Right: relationship between R_{sand} and $\Delta T_{10cm}/\Delta t$.

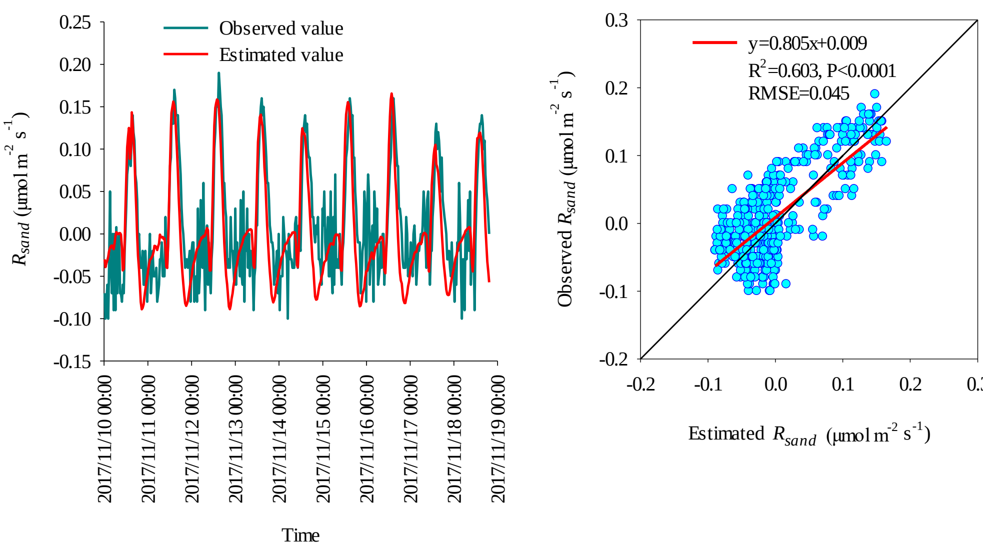

Figure 6. Comparison of R_{sand} obtained from experimental data and estimated by Equation 4 in

sand. Left: Time series of observed and estimated R_{sand}. Right: Regression relationship between observed and estimated R_{sand}.

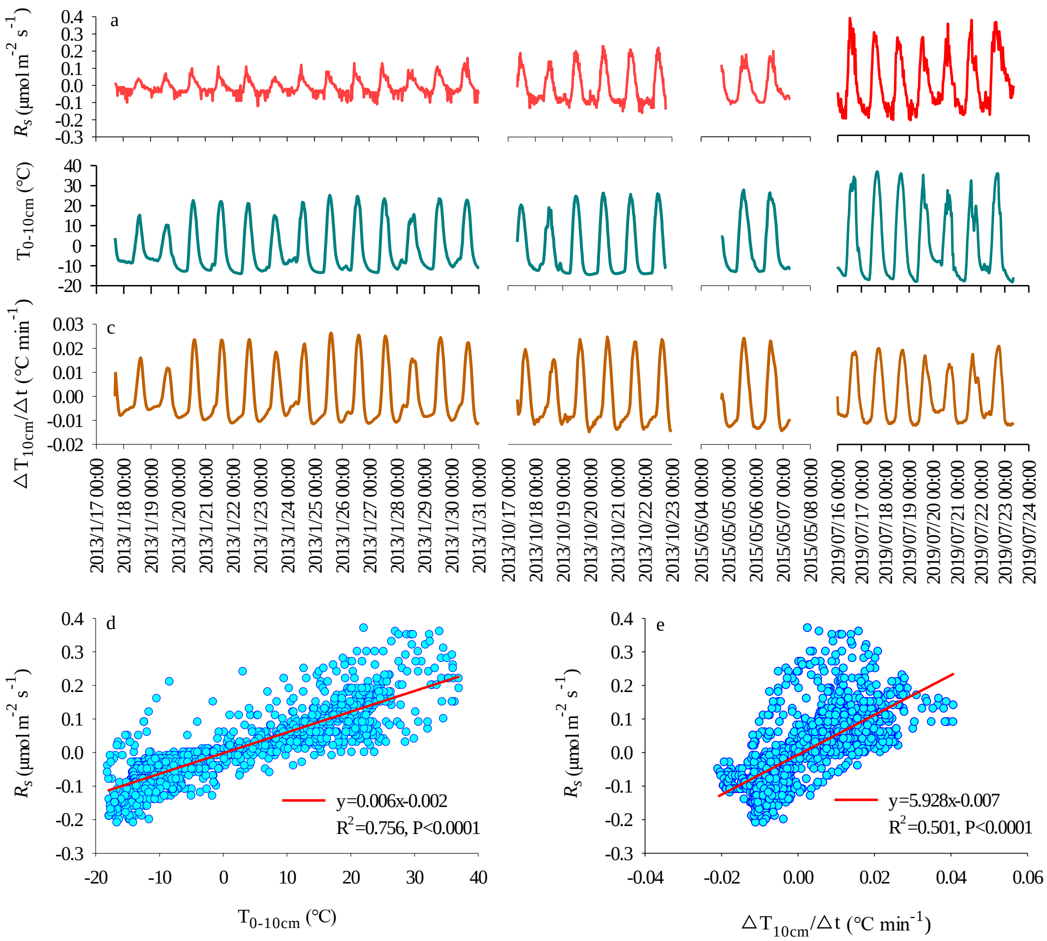

Figure 7. Relationships among $T_{0–10cm}$, $\Delta T_{10cm}/\Delta t$, and R_s during January 17–31, 2013, October 17–23, 2013, May 4–7, 2015, and July 16–23, 2019. a-c, Time series of (a) R_s, (b) $T_{0–10cm}$, and (c) $\Delta T_{10cm}/\Delta t$. d, Regression analysis between R_s and $T_{0–10cm}$. e, Regression analysis between R_s and $\Delta T_{10cm}/\Delta t$.

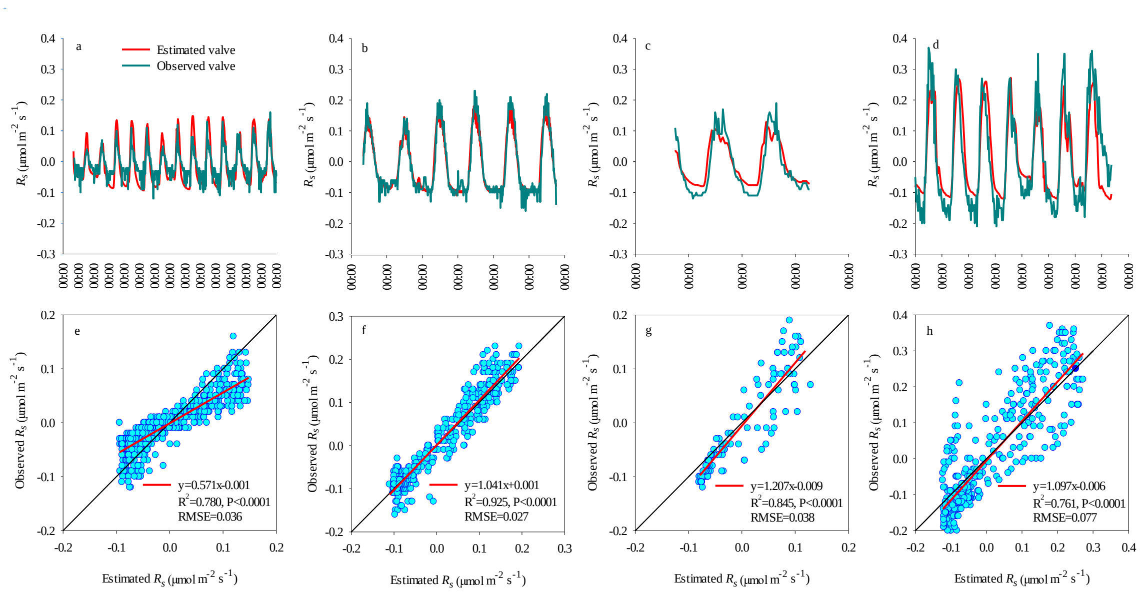

Figure 8. Comparison of R_s obtained from experiments and estimated by Equation 4 in shifting sand. a-d, Relationships between the observed and estimated R_s are shown for (a) January 17-31, 2013, (b) October 17-23, 2013, (c) May 4-7, 2015, and (d) July 16-23, 2019 and. e-h, The regression relationships for the time periods are shown in (a-d).

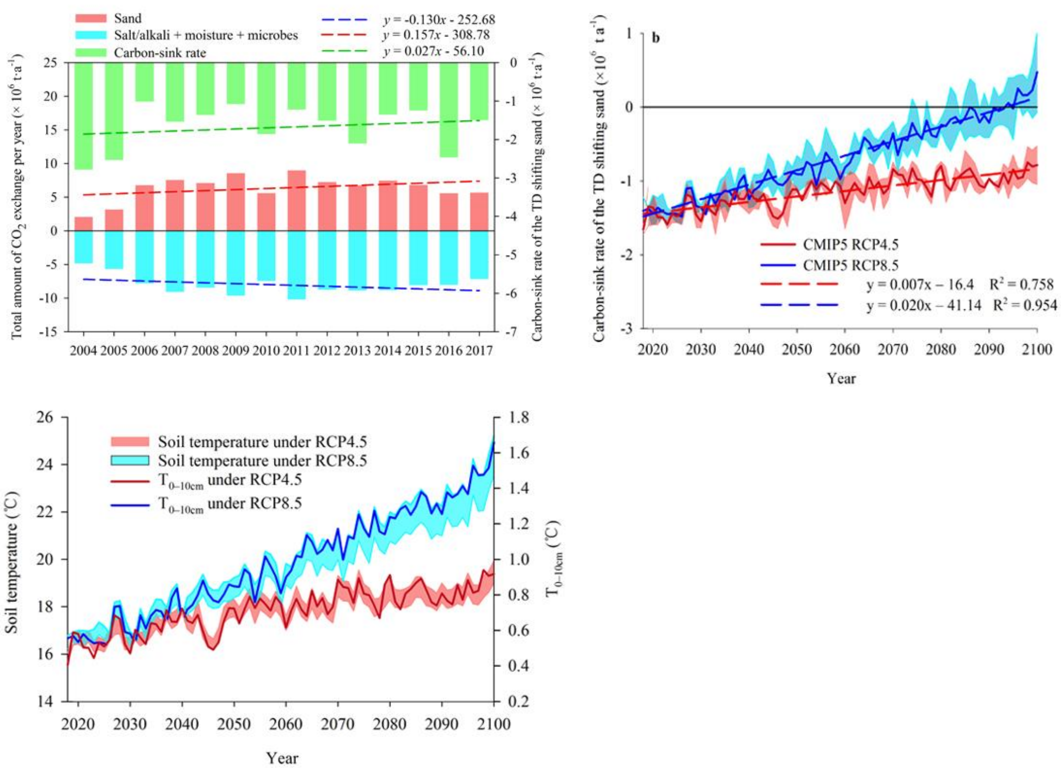

Figure 9. Temporal variation in the total amount of CO_2 exchange per year in the TD shifting sand. a, Temporal variation in the total amount of soil CO_2 exchange per year for 2004–2017 in

TD shifting sand. b, Under Representative Concentration Pathway (RCP) scenarios 4.5 and 8.5, temporal variation in the total amount of CO_2 exchange per year for 2018–2100 in TD shifting sand. Shading denotes the mean±standard deviation of three models (MIROC5, MRI-CGCM3, and CMCC-CMS). c, Temporal variations in soil temperature and $T_{0\text{-}10cm}$ under the RCP scenarios 4.5 and 8.5. The upper boundary of the shading denotes the soil temperature at 0 cm, and the lower boundary denotes the soil temperature at 10 cm.

Table 1. Description of the physical and chemical properties of the topsoil of the shifting sand in the hinterland of the Taklimakan Desert (TD) (mean ± standard deviation).

Variable	Depth (cm)	
	0–5	5–10
Average gravimetric soil moisture content (%, kg kg^{-1})	0.0013±0.0002	
Soil total salt (g kg^{-1})	3.45±0.35	9.64±1.10
Soil organic carbon (g kg^{-1})	0.56±0.12	0.63±0.03
Soil total nitrogen (g kg^{-1})	0.06±0.01	0.09±0.02
Ratio of soil organic carbon to soil total nitrogen	9.85±0.83	7.66±1.58
pH	7.33±0.02	7.3±0.04
Bacteria (organisms g^{-1} dry soil) (Gu et al., 2000)	20295	
Fungi (organisms g^{-1} dry soil) (Gu et al., 2000)	45	
Actinomyces (organisms g^{-1} dry soil) (Gu et al., 2000)	238	

Table 2. Methods of topsoil sample pretreatment.

Sample No.	Contribution of each component	Sample weight (kg)	Pretreatment method

1	R_s	13.21	No treatment
2	$R_{sand} + R_{water} + R_{salt/alkali}$	13.22	Sand samples were autoclaved to remove the contribution of soil microorganisms to the CO_2 flux. To ensure that sterilization was sufficient, autoclaving was repeated three times, each time for half an hour. The sterilized high-temperature sand was immediately placed in an oven for drying at 105 °C. The dried sand was sealed tightly before being placed in a sterile UV chamber. After allowing the sample to stand in a sterile state for 1 day, a watering can was used to add 17.18 ml of distilled water according to the soil water content measured in the field (0.0013 kg/kg). The sand sample was evenly mixed while the distilled water was added and was then sealed and allowed to stand for 2 days so that CO_2 and water in the sample could achieve equilibrium.
3	$R_{sand} + R_{water}$	12.23	First, collected sand samples were placed in plastic boxes before 30 L of distilled water was added to the samples. After fully mixing, the sample was allowed to stand for 1 hour, and the upper liquid layer was decanted. This procedure was repeated three times to sufficiently remove soluble salts and alkalis in the sand sample. Subsequently, the treatment method for Sample 2 (three rounds of sterilization, followed by drying, adding distilled water (15.9 ml), and being left to stand) was followed.
4	R_{sand}	12.33	The process was similar to Sample 3, but distilled water was not added.

Table 3. Synergistic effect analysis for R_{sand}/R_s with $T_{0–10cm}$ and $\Delta T_{10cm}/\Delta t$.

	No.	Fitted equation	R^2
R_{sand}	1	$R_{sand} = 0.007 + 0.002\ T_{0–10cm} + 2.958\ \Delta T_{10cm}/\Delta t$	0.496**
	2	$R_{sand} = –0.010 + 0.002\ T_{0–10cm} + 1.542\ \Delta T_{10cm}/\Delta t + 0.108\ T_{0–10cm}$	0.614**

		$\Delta T_{10cm}/\Delta t$	
	3	$R_{sand} = -0.031 - 0.002\ T_{0-10cm} + 4.116\ \Delta T_{10cm}/\Delta t + 0.0004\ T_{0-10cm}^{\ 2} - 67.961\ (\Delta T_{10cm}/\Delta t)^{2}$	0.748**
	4	Failed	/
R_s	1	$R_s = -1.55 \times 10^{-4} + 0.008\ T_{0-10cm} - 2.445\ \Delta T_{10cm}/\Delta t$	0.756**
	2	$R_s = 0.007 + 0.008\ T_{0-10cm} - 2.147\ \Delta T_{10cm}/\Delta t - 0.048\ T_{0\text{-}10cm}\ \Delta T_{10cm}/\Delta t$	0.768**
	3	$R_s = -0.004 + 0.006\ T_{0-10cm} - 0.194\ \Delta T_{10cm}/\Delta t + 3.669 \times 10^{-5}\ T_{0-10cm}^{\ 2} - 35.928\ (\Delta T_{10cm}/\Delta t)^{2}$	0.792**
	4	Failed	/

Notes: R^2 is the goodness-of-fit of the regression equation; '*' and '**' indicate a significant correlation at $P < 0.05$ and $P < 0.01$ (two-tailed), respectively. For R_{sand}, data from temperature-controlled experiments and field observations were combined to conduct the fitting analysis. For R_s, data from field observations were conducted the fitting analysis.